FlatChem 46 (2024) 100672

Contents lists available at ScienceDirect

FlatChem

journal homepage: www.sciencedirect.com/journal/flatchem

Direct laser writing of MnO_x decorated laser-induced graphene on paper for sustainable microsupercapacitor fabrication

Rodrigo Abreu [a], Maykel dos Santos Klem [a,b], Tomás Pinheiro [a], Joana Vaz Pinto [a], Neri Alves [b], Rodrigo Martins [a], Emanuel Carlos [a,*], João Coelho [a,c,*]

[a] CENIMAT|i3N, Departamento de Ciência de Materiais, Faculdade de Ciências e Tecnologia, Universidade Nova de Lisboa and CEMOP/UNINOVA, Campus da Caparica, Caparica 2829-516, Portugal
[b] School of Technology and Sciences, São Paulo State University (UNESP), Presidente Prudente, SP 19060-900, Brazil
[c] Departamento Física de la Materia Condensada and Instituto de Ciencia de Materiales de Sevilla, Universidad de Sevilla−CSIC, Avenida Reina Mercedes s/n, 41012 Sevilla, Spain

ARTICLE INFO

Keywords:
Laser-induced graphene
Microsupercapacitor
Paper-based devices
Manganese oxide doping
Flexible electronics

ABSTRACT

Laser-induced graphene (LIG) on paper is a popular choice for fabricating flexible micro-supercapacitors (MSCs) as it is a simple and sustainable process. However, carbon-based MSC electrodes have limited energy densities. To address this challenge, this study presents a highly reproducible and cost-effective method for decorating manganese oxide (MnO_x) on interdigital LIG MSC electrodes, fabricated via a single-step direct laser writing (DLW) process on paper substrates. The paper fibers embedded with MnO_x precursors are transformed into graphene through laser processing while reducing the salt, resulting in the formation of MnO_x-LIG. The resulting MnO_x-LIG-MSC exhibits a specific capacitance of 12.30 mF cm^{-2} (0.05 mA cm^{-2}) with a 60 % retention at 1000 bending cycles (30°), due to the pseudocapacitive contribution of MnO_x. Furthermore, the devices exhibit high electrochemical stability, retaining 190 % of the initial specific capacitance after 10,000 cycles, and a high energy density of 2.6 μWh cm^{-2} (at a power of 0.109 mW cm^{-2}). The study demonstrates that manganese oxide-based LIG-MSCs have the potential to be used as energy storage devices for portable, low-cost, and flexible paper electronics.

Introduction

The growing prevalence of portable and wearable technologies has prompted a surge in demand for enhanced energy storage and harvesting systems [1–3]. While lithium-ion batteries (LIBs) possess certain limitations, including their size, hazardous electrolytes, and reliance on scarce lithium, supercapacitors offer a compelling alternative for such applications [4]. Micro-supercapacitors (MSCs) are worthy of particular attention due to their high power density, extended life cycles, rapid charge–discharge capabilities, and straightforward design [5–8]. In addition, the planar interdigital configuration of MSCs offers flexibility, lightness, and ease of packaging, distinguishing them from traditional rigid metal-based designs [5,9]. Furthermore, the fabrication of MSCs on sustainable substrates, such as paper, wood, cork, and cotton, represents an environmentally conscious solution to the growing problem of electronic waste [10–12]. For instance, Shan *et al.* developed wood-based hierarchical porous nitrogen-doped carbon/manganese dioxide composite supercapacitor electrodes by following a route of carbonization and KOH activation of cedar branches [13]. The obtained device exhibited a specific capacitance of 162.4 F g^{-1} at 0.5 A g^{-1}, along with remarkable stability. In the specific case of paper, various techniques have been employed to fabricate MSCs, with direct laser writing being one of the most promising approaches [14–18]. Laser processing transforms cellulosic paper fibers into a three-dimensional porous graphene foam, known as laser-induced graphene (LIG) [10–12,19]. LIG has several advantages for supercapacitors, including its large surface area, which enables increased energy storage capabilities, improved capacitance, and energy density. Furthermore, graphene's exceptional electrical conductivity allows for rapid charge and discharge rates, making it ideal for high-performance supercapacitor applications. LIG processing has several advantages, including one-step patterning, reproducibility, minimal waste generation, and operational simplicity

* Corresponding authors at: CENIMAT|i3N, Departamento de Ciência de Materiais, Faculdade de Ciências e Tecnologia, Universidade Nova de Lisboa and CEMOP/UNINOVA, Campus da Caparica, Caparica 2829-516, Portugal.
E-mail addresses: e.carlos@fct.unl.pt (E. Carlos), jmesquita@us.es (J. Coelho).

https://doi.org/10.1016/j.flatc.2024.100672
Received 13 February 2024; Received in revised form 26 April 2024; Accepted 11 May 2024
Available online 16 May 2024

[11–14]. Coelho *et al.* [14] introduced a method for producing LIG on paper with a sheet resistance of 30 Ω sq^{-1} and an improved electrode/electrolyte interface. In this case, LIG was used as both an electrode and current collector for micro-supercapacitors. It achieved specific capacitances of 4.60 mF cm^{-2} at 0.015 mA cm^{-2} and exhibited cycling stability exceeding 10,000 cycles at 0.50 mA cm^{-2} [14]. Micro-supercapacitors based on carbon are a type of electric double-layer capacitors (EDLCs) that have high power densities and fast charge/discharge rates. However, EDLCs have lower specific capacitances and energy densities than pseudocapacitors, such as metal oxides which include some examples like RuO_2, NiO, CuO, and Co_3O_4, while MnO_x is the most promising material for electrochemical capacitors due to its low cost, non-toxicity, abundance, environmental friendliness, and high theoretical capacitance [20–22]. This is because the charge storage mechanism in EDLCs is based on electrostatic attraction, while the charge storage mechanism in pseudocapacitors is based on fast redox reactions [23]. By using metallic precursors like metal salts or metal-containing compounds, it is possible to achieve a metal oxide-impregnated LIG film. This technique involves depositing a solution of the desired dopant onto a substrate, allowing it to evaporate and form a thin film. Then, laser-induced heating can cause the precursor to undergo thermal decomposition, leading to the release of volatile species and the formation of metal oxide nanoparticles. At the same time, the graphene structure formed upon lasing acts as a support for the nanoparticles, enhancing their stability and preventing agglomeration [24–26].

This work presents a simple method for enhancing the performance of paper-based MSCs by integrating pseudocapacitive metal oxide particles into the device structure. In particular, manganese acetate, a manganese precursor, was deposited onto paper and converted into oxide under laser irradiation. Through a singular procedural step, a MnO_x-LIG composite material was synthesized, leveraging the synergistic benefits of both components. The resulting composite, when employed as electrodes for MSC, exhibited an appreciable specific capacitance of 12.30 mF cm^{-2} (0.05 mA cm^{-2}). Notably, even after subjecting the material to 1000 bending cycles (30°), it demonstrated a retention rate of 60 %. This resilience can be attributed to the pronounced pseudocapacitive effects induced by the MnO_x component. The underlying theoretical framework suggests that the synergistic combination of MnO_x and LIG promotes enhanced electrochemical performance. MnO_x contributes to the overall capacitance by facilitating pseudocapacitive charge storage, while LIG, with its unique porous and conductive nature, provides a favorable substrate for efficient charge transport. Moreover, the fabricated devices exhibited outstanding cycling stability, retaining a considerable capacitance of 23.33 mF cm^{-2} over an extensive span of more than 10,000 cycles. This longevity is indicative of the robust structural integrity and durability of the MnO_x-LIG composite under cyclic electrochemical stresses. In terms of energy storage metrics, the devices exhibited a commendable energy density of 2.6 μWh cm^{-2} and a power density of 0.109 mW cm^{-2}. These results demonstrate the promising potential of the MnO_x-LIG composite as a high-performance material for energy storage applications, aligning with theoretical expectations rooted in the combined benefits of MnO_x and LIG in facilitating advanced electrochemical processes.

Materials and methods

Paper substrate treatment and wax printing

Commercial paper sheets of Whatman™ type 1 (Cytiva) were soaked in 0.1 M sodium tetraborate decahydrate (≥99.5 %, Sigma-Aldrich) for 15 min and proceeded to dry overnight. Wax was printed onto the prepared substrates using a Xerox ColorQube 8580DN printer [10]. For the laser parameter matrix and LIG electrodes, the substrate was then heated at 100 °C on a heating plate for approximately 1 min. For manganese acetate precursor solution on LIG electrodes, two diffusion layers of wax with a non-diffused layer on the top and a fully closed non-diffused layer on the bottom were applied. Also, on the top side, a blank well measuring 2 cm × 3 cm was designed for the deposition of the manganese acetate.

Laser parameters and matrix fabrication

For the LIG matrix, squares measuring 0.5 cm × 0.5 cm, were engraved onto treated paper using a 10.6 μm CO_2 laser system (VLS 3.50, Universal Laser Systems) at various power and speed settings, as shown in Figure S1, ranging from 1.5 W to 4.5 W and 38.1 cm s^{-1} to 127 cm s^{-1}, respectively. Before engraving, the paper substrates were flattened and placed on a 1.1 mm thick glass surface. The experiments were conducted under ambient conditions without nitrogen flow, using a beam diameter of 0.127 mm (2.0 lens) and a pulse rate of 1000 pulses per inch at a focal height of 2.54 mm. Ultrapure Milli-Q water laboratory grade (conductivity < 0.1 μS cm^{-1}) was utilized to prepare all solutions. All chemicals were used as purchased.

MnO_x impregnation and LIG-MSC on paper fabrication

An aqueous solution of manganese acetate (1 M, $C_4H_6MnO_4$) was prepared and then 100 μl was dropped into the paper well and left to dry overnight.

The interdigital micro supercapacitor electrodes were then produced having an area of 1.86 cm in length and 1.67 cm in width. The fingers of the electrodes have a fixed interspacing distance of 0.06 cm and dimensions of 0.96 cm x 0.05 cm. The pads of the electrodes, which measure 0.5 cm x 0.5 cm, were coated with silver paste and allowed to cure at 40 °C on a hotplate for 15 min. The fabrication of the MSC was conducted under ambient conditions without nitrogen flow, using a beam diameter of 0.127 mm (2.0 lens) and a pulse rate of 1000 pulses per inch at a focal height of 2.54 mm with a 6 % power and 6 % speed.

LIG and LIG-MnO_x characterization

Morphological and structural analysis of the materials was carried out using a Hitachi High Technologies tabletop SEM microscope TM3030 Plus Hitachi, with an acceleration voltage of 15 kV. The structural characterization was performed using Raman Spectroscopy. For this purpose, a Renishaw® inViaTM Qontor® confocal Raman microscope equipped with a Renishaw Centrus 2957 T3 detector, and a 532 nm laser (green) operating at 10 mW was used. A 50x magnification Olympus objective lens (Olympus) was used to focus the laser beam. All measurements were carried out with three scans of 10 s laser exposure. To analyze the chemical and phase compositions of the samples, an XPS/UPS Kratos Axis Supra was used operating at 225 W with a monochromatized (1486.60 eV) A1 Kα. A pass energy of 20 eV was employed for more thorough scans and 160 eV for wider scans. To measure the sheet resistance of the LIG, the four-point probe method was used with a Biorad/Nanometrics HL5500, at room temperature, and three samples of each condition were measured.

Electrolyte fabrication and MSC electrochemical characterization

A PVA/LiCl aqueous gel was used as an electrolyte. 1 g of PVA was dissolved in 10 mL of distilled water at 90 °C with mechanical stirring for 1 h. After that, 2.2 g of LiCl was mixed in for another hour. Before the electrolyte casting, the microsupercapacitor electrodes produced in 2.3 were exposed to UV light at 15 cm height (NOVASCAN–PSD Pro Series Digital UV Ozone System) for 15 min at room temperature. 20 μl of electrolyte was then cast onto the devices. The assembled micro-supercapacitors were allowed to dry at room temperature overnight. LIG-MSC electrochemical performance was studied in a BioLogic SP-50 potentiostat. The scan rates used for the cyclic voltammetry (CV) were 10, 30, 50, 100, 300, 500, and 1000 mV s^{-1} and for the galvanostatic charging/discharging (GCD), the current density values used were 20,

30, 40, 50, and 100 μA cm^{-2}. Electrochemical impedance spectroscopy (EIS) was performed using a sinusoidal potential input with an amplitude of 10 mV and a frequency range of 1 Hz to 100 MHz in a PalmSens4 potentiostat.

The fabricated MSCs specific areal capacitance, C_A (mA), can be determined by analyzing the charge–discharge curves as expressed by:

$$C_A = \frac{I\Delta t}{A\Delta V} \quad (1)$$

Where the parameters are the applied current (I in mA), discharge time (Δt *in seconds*), active area of the MSC (A in cm^2), and potential difference (ΔV in Volts) between the initial potential (V2) at the beginning of discharge, accounting for the IR potential drop, and the final potential (V1) at the end of discharge.

The following equation was used to calculate the energy density (E_D in μWh cm^{-2}):

$$E_D = \frac{1}{2} \times C_A \times V^2 \quad (2)$$

Where C is the specific aerial capacitance and V is the voltage window. A factor of 3600 was used to convert Joules to Wh. The power density (P_D in mW cm^{-2}) was determined considering the discharge time (Δt) obtained from the galvanostatic charge–discharge (GCD) plot:

$$P_D = \frac{E_D \times 3600}{\Delta t} \quad (3)$$

Results and discussion

MSC electrodes processing and optimization

Fig. 1 summarizes the workflow for MSC fabrication in this project, which is based on two main fabrication routes.

Route 1 (red line) for the fabrication of bare LIG-based MSC without any metal precursor, which acts as a control sample. Route 2 (blue line) corresponds to the actual route for the fabrication of LIG-MnO_x supercapacitors. For both routes, before laser engraving, the paper substrates are soaked in sodium tetraborate solution, which acts as a fire-retardant agent. Due to their cellulose-based composition, paper substrates are susceptible to total ablation or thermal degradation, even with low laser power. Laser exposure can raise the substrate temperature above 2000 °C, whereas cellulose ignites at around 230 °C [13]. As such, the preliminary treatment with sodium tetraborate is key for the processing of the samples [8]. Then, for Route 1, the paper substrate is coated with a hydrophobic wax layer, to contain the electrolyte diffusion throughout the paper and eventually deteriorate its mechanical properties [10]. Then, a CO_2 laser engraver was employed to create the power/speed matrix with the parameters described in the methods section. A sample matrix and subsequent LIG characterization are provided in the supplementary information (Figure S1). It was observed that under optimal conditions LIG sheet resistance can be as low as 24 ± 3 Ω sq^{-1} (Figure S2). These values agree with the previous LIG on paper studies and as such, the processing conditions will be used for route 2 [10,14,16]. Finally, interdigitated electrodes are fabricated and exposed to a UV treatment to enhance the wettability of the LIG sample. Gel electrolyte is then deposited on the fingers, finalizing the MSC fabrication process.

For Route 2, after the sodium tetraborate pre-treatment, 100 μL of an aqueous solution of manganese acetate (MnO_x precursor) was drop cast on the substrates. However, the hydrophobic nature of the waxed substrate forbids the deposition of the manganese acetate MnO_x precursor solution. As shown in Fig. 2, to cover this issue and to avoid the spread of electrolytes, various wax diffusions on paper were applied.

Two diffusions showed little to no internal liquid spreading, keeping the precursor solutions in a very well-defined well. As seen from Fig. 2, a portion of the substrate's top side is not waxed. This square well of 2 cm x 2 cm was kept for the deposition of the precursor solution and laser

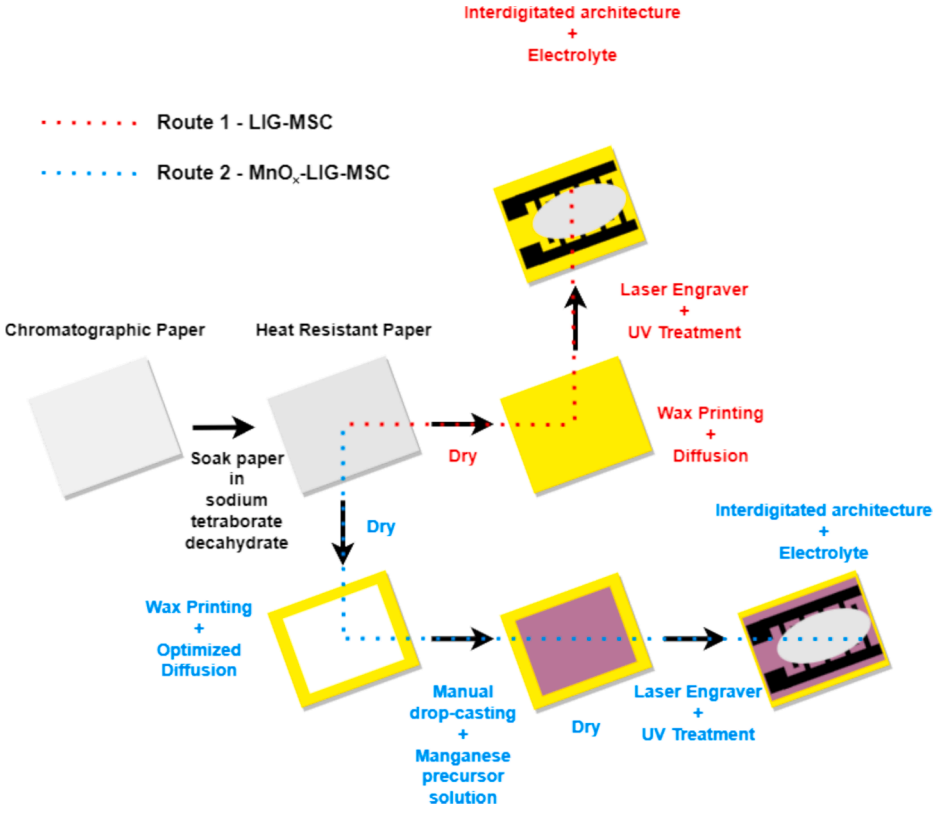

Fig. 1. LIG-MSC and MnO_x-LIG-MSC fabrication process; Route 1) Step-by-step process to fabricate the LIG-MSC and Route 2) Step-by-step process to fabricate the MnO_x-LIG-MSC.

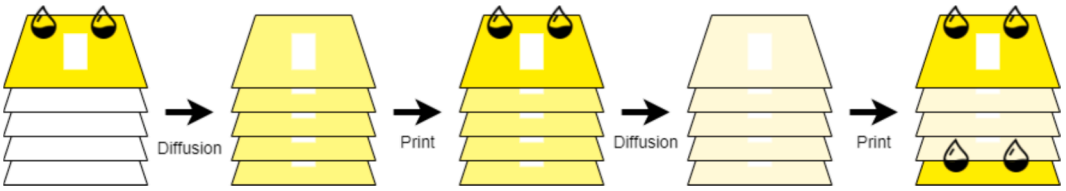

Fig. 2. Schematic of internal paper layers with a two-wax diffusion process.

processing at the optimized conditions. Wax was deposited on both the top and bottom of the paper without diffusion to further prevent solution spreading. After this initial step, and following the procedure in Fig. 1, the substrates were laser irradiated at optimized conditions to prepare MnO_x impregnated LIG samples. On the other hand, while measuring the sheet resistance of the MnO_x-LIG-MSC, the value increases to 52 ± 3 Ω sq^{-1} which is explained by the fact more Mn atoms are being added to the system.

MnO_x induction and Electrical, Morphological, and structural characterization of the MnO_x-LIG composite on paper

The morphological characterization of the prepared samples was studied by electron microscopy. The SEM micrograph in Fig. 3a revealed the presence of a fibrous open structure, which is characteristic of LIG on paper. On the contrary, the paper surface reveals a densely packed network of cellulose fibers with a distinct fibrous structure as can be seen in Figure S3. The high magnification exposes individual fiber details, showcasing their intricate patterns and surface irregularities. Fig. 3b and Fig. S3d show the borderline between non-processed and processed areas of the substrate and as it can be seen, unprocessed paper exhibits a much more compact structure in comparison to LIG. It is also possible to observe that the boundary between processed and unprocessed areas is very well defined due to the high spatial resolution of the laser. As such an abrupt change in the media properties is observed, rather than a gradual transition as it could be expected from a photothermal process.

Some crystals can be observed on the processed area which might be an indication of MnO_x being formed along with LIG. In Fig. 3c it is shown the graphical results from energy-dispersive X-ray spectroscopy (EDS) analysis. A uniform distribution of Mn, O, and C is observed suggesting that the MnO_x phases are well distributed throughout the paper substrate, which is essential for the effective functioning of the capacitor. In Fig. 3d it shows the relative mass percentage of the elements present in the sample. As expected, most of the sample (79 %) is composed of carbon derived from the LIG and the substrate. The presence of manganese (4.5 %) and oxygen (16.5 %) can be attributed to the MnO_x formation. However, some of the oxygen is residual from the lasing process. When paper is processed, most of the oxygen in its structure is released in the gas plume, but not in its entirety [27]. Therefore, a direct correlation between the percentages of Mn and O is not established. To better understand the type of manganese species that are present in the irradiated sample, XPS and Raman spectroscopy analyses were performed and presented in Fig. 4.

As shown in Fig. 4a, the XPS spectrum exhibits the Mn $2p_{3/2}$ peak at 653.5 eV representing the binding energy of the Mn $2p_{3/2}$ electrons in the outermost shell of the Mn atoms. The Mn $2p_{1/2}$ peak at 642.1 eV is

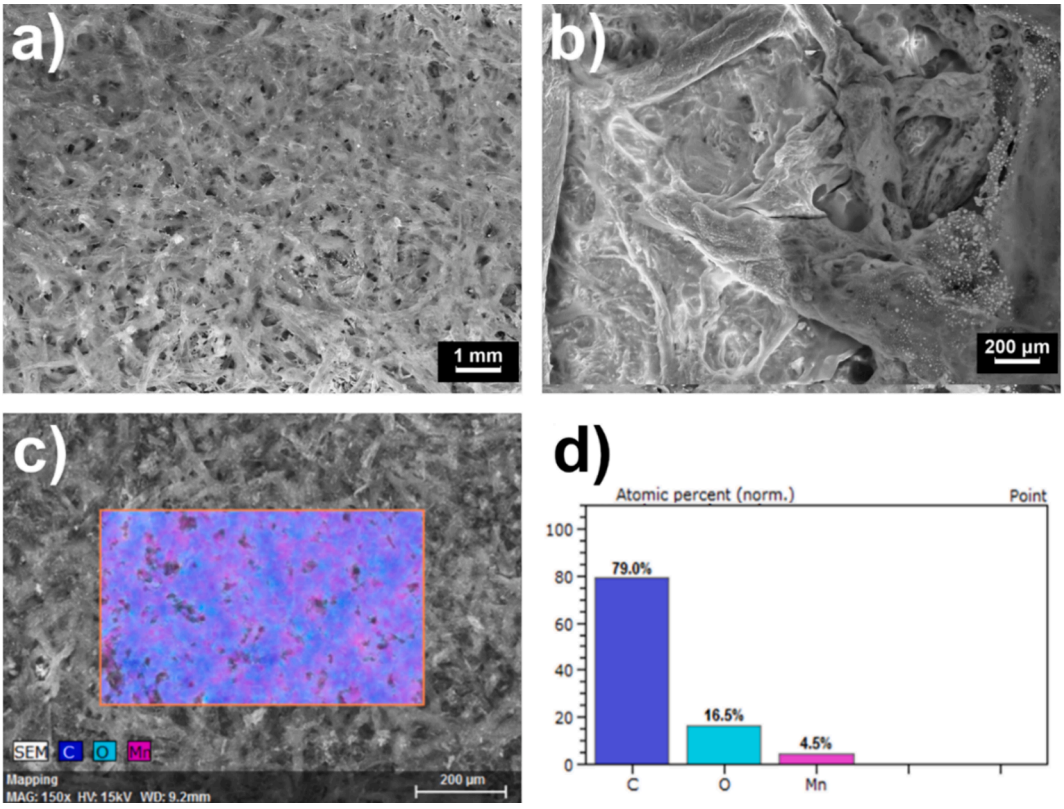

Fig. 3. SEM and EDS images of the MnO_x impregnated LIG processing samples on paper soaked with manganese acetate; a) 150x magnification; b) border of the LIG – paper on the left and LIG on the right with 1000x magnification; c) EDS analysis of the SEM image; d) Elemental composition.

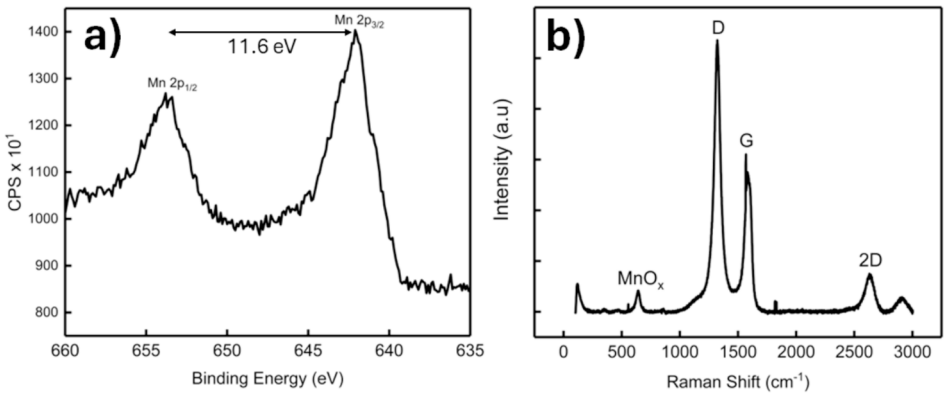

Fig. 4. MnO_x-LIG a) XPS with emphasis on the Mn $2p_{1/2}$ and Mn $2p_{3/2}$ peaks; b) Raman spectra portraying the commonly seen D, G, and 2D characteristic peaks of LIG and the MnO_x highlighting the presence of this molecule. The spectra for bare LIG XPS and Raman, are shown in Supplementary information as Fig. S4a and S4b, respectively.

typically observed at a lower binding energy than the Mn $2p_{3/2}$ peak. The energy difference between the two peaks (11.6 eV) is due to spin–orbit splitting and it is characteristic of MnO_x samples [28,29]. To further understand the nature of the phases present in the sample, the XPS spectrum was deconvoluted to determine the chemical valence band of Mn present in the sample (Figure S5). It is possible to observe that MnO_x-LIG is mainly composed of Mn^{4+} and Mn^{3+} species, corresponding to MnO_2 and Mn_3O_4 [26,30,31]. These observations are in good agreement with a model proposed for the photothermal conversion of the natural precursors into LIG [31]. The substrates absorb the laser beam energy and promote the heat transfer, followed by the oxidation of the precursor into MnO_2 and Mn_3O_4:

$$2Mn(CH_3COO)_2.4H_2O \rightarrow MnO + 4CO_2 + 7H_2O \quad (1)$$

$$2MnO + O_2 \rightarrow 2MnO_2 \quad (2)$$

$$2MnO + MnO_2 \rightarrow Mn_3O_4 \quad (3)$$

The proposed model corroborates the obtained results, validating the presence of multiple phases of manganese oxides on the samples, and as such they are referred to as MnO_x, rather than MnO_2 [26,31]. The Raman spectrum in Fig. 4b further corroborates the XPS results. The graph presents the characteristic D, G, and 2D peaks of graphitic carbons (Fig. S4b) [32–34]. Additionally, the peak at 640 cm^{-1} is typically attributed to the Mn-O bending mode in MnO_x, whereas the peak at 518 cm^{-1} is associated with the Mn-O stretching mode [35]. Further MnO_x-LIG characterization was conducted by XRD (Figure S6). The paper substrate exhibits clear and well-defined peaks that corresponds to cellulose semi-crystalline structure and that do not change after laser irradiation. LIG is not known for exhibiting a characteristic XRD profile. The MnO_x-LIG sample reveals the presence of very low intense peaks at 2θ (30.45°, 40.50° and 58.67°) that may be attributed to the (1 1 1), (2 0 0) and (2 2 0) reflections of a face-centred cubic MnO phase (JCPDS Card 00–075-1090). Due to the low intensity signal, mainly masked by the paper substrate we cannot discard the presence of other MnO_x mixtures.

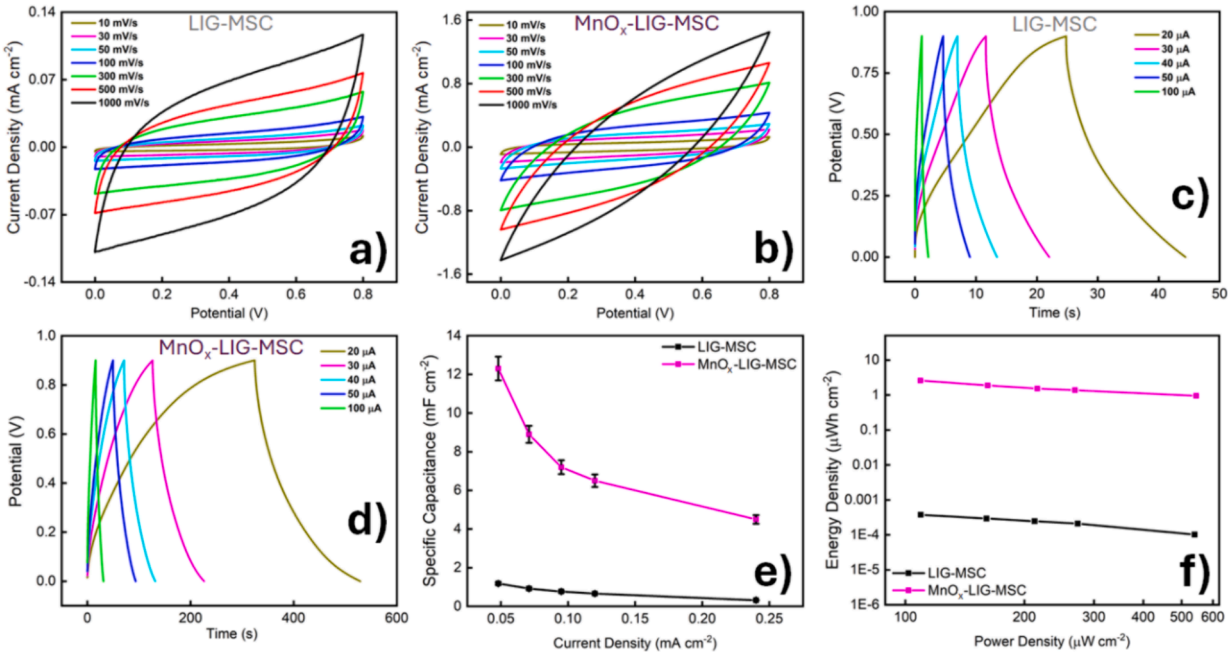

Fig. 5. Cyclic voltammetry, specific capacitance, galvanostatic charge–discharge and energy density curves of a) LIG-MSC CV; b) MnO_x-LIG-MSC CV; c) LIG-MSC GCD; d) MnO_x-LIG-MSC GCD e) Specific capacitances of LIG-MSC (black) and MnO_x-LIG-MSC (magenta) and f) Ragone plot demonstrating the Energy Density by Power Density for both LIG-MSC (black) and MnO_x-LIG-MSC (magenta).

Fabrication and electrochemical testing of the MnO_x-LIG microsupercapacitors

After confirming the presence of MnO_x on the LIG structure, the laser was used to create interdigital MSC patterns (Figure S8 and Table S2) on the paper substrates under optimized conditions as shown in Route 2 of Fig. 1. Cyclic voltammetry (CV) experiments were conducted on both LIG-MSC and MnO_x-LIG-MSC and the results are shown in Fig. 5a and 5b, respectively. CV curves usually exhibit rectangular loops, which are a common characteristic of graphene-based supercapacitors [36,37].

Given manganese oxide's pseudocapacitive nature, the MSC charge storage mechanism derives as well from reversible redox reactions occurring at the electrode surface [38,39]. As such, the MnO_x-LIG-MSC exhibits a heightened current response compared to the LIG-MSC, reinforcing the pseudocapacitive nature of manganese oxide [40]. Examining Fig. 5c, the triangular shape of the LIG-MSC corresponds to a capacitive energy-storage mechanism involving the formation of a double layer at the electrode–electrolyte interface [17,41,42]. Fig. 5d shows a similar curve for MnO_x-LIG-MSC. However, the larger charging and discharging times signal the presence of a pseudocapacitive energy-storage mechanism attributed to surface-controlled redox reactions of MnO_x [43]. This effect is further reflected in terms of capacitances as shown in Fig. 5e where the addition of MnO_x to the carbon-based matrix leads to a specific areal capacitance increase of around ten times. In more detail, the LIG-MSC exhibits a specific capacitance of 1.18 mF cm^{-2} at a current density of 0.05 mA cm^{-2}. However, with an increase to 0.24 mA cm^{-2}, the specific capacitance decreases to 0.32 mF cm^{-2}, indicating a diminishing energy storage efficacy at higher current densities. In striking contrast, MnO_x-LIG-MSC, which, at 0.05 mA cm^{-2}, has a specific capacitance of 12.30 mF cm^{-2}. Yet, at 0.07 mA cm^{-2}, the specific capacitance drops to 8.90 mF cm^{-2}, highlighting a faster decline when compared to the LIG-MSC. This decline is attributed to the slower kinetics at elevated current densities, which are characteristic of pseudocapacitors. However, MnO_x enhances the electrode's effective surface area, contributing to increased capacitive behavior and higher capacitance [44]. Examining Fig. 5f, the introduction of MnO_x to the MSCs enhances energy density due to its pseudocapacitive activity. To sum up, the electrochemical performance of the produced MSCs is in line with literature reports based on LIG electrodes and other porous materials [24,26,31]. These observations are further confirmed by EIS analysis available at the SI (Figure S7).

The endurance of the MSC was also tested by performing cycling experiments and bending tests as presented in Fig. 6.

Fig. 6a illustrates cyclability tests for 10,000 cycles at a current of 100 μA with a voltage potential of 0.8 V. Coelho *et al.* have shown that paper-based LIG microsupercapacitors exhibit excellent cycling stability (>10,000 cycles at 0.5 mA cm^{-2}) retaining about 85 % of their initial capacitance [14]. The results for MnO_x-LIG-MSC indicate that the capacitor performance improved by approximately 190 % with cycling. This improvement may be attributed to the formation of a more effective electrolyte/electrode interface or activation of additional electrochemically active sites on the electrode surface. Although such significant capacitance retention increases are uncommon, previous studies have reported them. For example, Hsiao *et al.* reported a 150 % increase in the performance of carbon nanomaterials/iron oxide/nickel–iron layered double hydroxides electrodes after 3200 cycles [45]. Similar results have been observed for LIG MSCs on cork,[16] asymmetric MSCs based on conductive polymer nanocomposite and activated carbon,[46] InSe/CNT thin film battery electrodes,[47] printed MXenes MSC on paper, [48] and carbonized bamboo fibers based MSCs [49]. It is widely accepted that the surface of highly porous and interconnected structures may become more accessible and in better contact with the electrolyte after repeated charge–discharge cycling. This provides a greater number of pores and surface area for double-layer formation and eventual electrochemical reactions to occur [16,47,49]. Despite the behavior observed for the cyclability tests, the coulombic efficiency (CE) reached 97 % after 10,000 cycles (Figure S9). Although values closer to 100 % are preferred, CE on the range 95 % to 100 % have been reported and regarded as an acceptable coulombic efficiency [50,51]. In the specific case of MnO_x-LIG-MSC, as the capacitance was not yet stable, it is possible that CE increases after more cycles.

In Fig. 6b, subjecting the MnO_x-LIG-MSC to 1000 bending cycles at 30° reveals a 60 % retention of its initial capacitance. For the bare lig electrodes on paper, a similar result was verified, mostly for the first bending cycles. This is a less-than-ideal result, however, the harsh mechanical tests employed may represent real-life situations. Additionally, for practical applications, the devices have to be encapsulated to protect the active material and avoid electrolyte loss. As such, these results along with the remaining electrochemical analysis demonstrate the capabilities of MnO_x-LIG-MSC as a flexible or conformable energy storage device".

The rise of portable and wearable technologies has fueled the need for better energy storage and harvesting systems [52,53]. Notably, MSC's planar interdigital configuration offers flexibility, lightness, and easy packaging, setting it apart from traditional metal-based designs [5,9,52,53]. LIG has attracted a lot of attention due to its simplicity and eco-friendly nature. Table 1, a detailed comparison between LIG MSCs produced on various substrates, different production methods, and dopants.

MnO_x-LIG-MSC demonstrates a competitive balance across key parameters, making it a highly promising electrode material for flexible micro-supercapacitors. With a specific capacitance of 12.30 mF cm^{-2}, MnO_x-LIG-MSC ensures efficient charge storage, catering to the demands of various applications. An energy density of 2.6 μWh cm^{-2} indicates effective energy storage in line with similar flexible micro-supercapacitors. A power density of 0.109 mW cm^{-2} positions MnO_x-LIG-MSC as a reliable choice for both quick energy delivery and sustained energy storage. Moreover, the cost-effective processing of MnO_x-

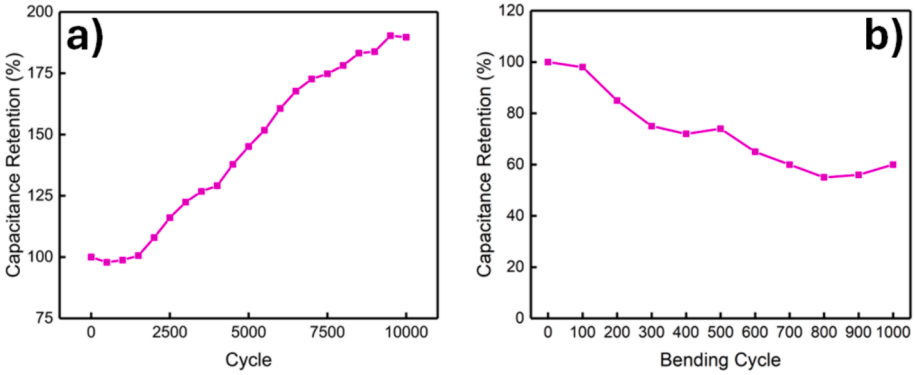

Fig. 6. MnO_x-LIG-MSC: a) Cyclability curve and b) Capacitance retention after 1000 bending cycles .

Table 1
List of different LIG-based MSCs reported on literature along with relevant electrochemical properties.

Device	Electrode Material	Dopant	Spec. Capacitance (mF cm^{-2})	Energy Density× (μWh cm^{-2})	Power Density (mW cm^{-2})	Cycle Stability (10,000 cycles)	Ref.
MnO_x-LIG-MSC	LIG	MnO_x	12.30	2.6	0.109	23.33 mF cm^{-2}	This work
LIG-MWCN	Carbon Nanotubes	–	6.09	3.4	0.199	–	[54]
LIG-Based	LIG	–	4.6	0.3	0.005	4.46 mF cm^{-2}	[14]
LIG-HS	LIG	Polyimide	0.650	–	–	0.624 mF cm^{-2}	[55]
Ni@ASC	LIG	Nickel Acetylacetonate	110	41.6	136	–	[56]
MnO_x/LIG NP	LIG-NP	MnO_x	15.04	1.22×10^3	1.278	–	[26]
MnO_x/graphene-PEK	LIG	MnO_x	48.9	3.1	2.5	46.11 mF cm^{-2}	[24]

LIG-MSC, utilizing easily accessible materials like paper and manganese oxide, enhances its economic viability. Its flexibility and portability make it a versatile candidate for various applications in flexible, low-cost, and portable electronics.

Conclusions

This study underscores the potential of paper-based impregnated Laser-Induced Graphene (LIG) as an advantageous material for flexible micro-supercapacitors due to its cost-effectiveness and facile processing. The incorporation of a manganese precursor during the paper substrate soaking, followed by laser processing, results in LIG adorned with a pseudocapacitive material, thereby augmenting the overall capacitance of the MSC. Optimal outcomes demonstrate that the addition of MnO_x leads to higher specific capacitances. The MnO_x-LIG-MSC exhibits formidable cycling stability, with a capacity retention of approximately 190 % which corresponds to 23.33 mW cm^{-2} sustained over > 10,000 cycles, coupled with a noteworthy energy density of 2.6 μWh cm^{-2} at 0.109 mW cm^{-2}. These findings affirm that MnO_x decoration on an interdigital MSC design is an effective strategy for enhancing supercapacitor performance. In essence, paper-based MnO_x-LIG-MSCs can serve as energy storage devices for flexible, cost-effective, and portable electronics, easily adaptable to various circuits and applications with diverse power requirements.

CRediT authorship contribution statement

Rodrigo Abreu: Resources, Project administration, Funding acquisition. **Maykel dos Santos Klem:** Investigation. **Tomás Pinheiro:** Writing – review & editing, Methodology. **Joana Vaz Pinto:** Writing – review & editing, Supervision, Resources, Project administration, Funding acquisition. **Neri Alves:** Writing – review & editing. **Rodrigo Martins:** Resources, Project administration, Funding acquisition. **Emanuel Carlos:** Writing – review & editing, Supervision, Resources, Project administration, Funding acquisition. **João Coelho:** Writing – review & editing, Visualization, Validation, Supervision, Resources, Project administration, Methodology, Funding acquisition, Formal analysis, Data curation.

Declaration of competing interest

The authors declare that they have no known competing financial interests or personal relationships that could have appeared to influence the work reported in this paper.

Data availability

Data will be made available on request.

Acknowledgments

This work was financed by national funds from FCT - Fundação para a Ciência e a Tecnologia, I.P., in the scope of the projects LA/P/0037/2020, UIDP/50025/2020 and UIDB/50025/2020 of the Associate Laboratory Institute of Nanostructures, Nanomodelling and Nanofabrication – i3N, Individual Call to Scientific Employment Stimulus – 2nd Edition (CEECIND/00880/2018) and the project GAMBIT (2022.01493.PTDC). This work was also partially supported by the European Union's Horizon Europe research and innovation program under grant agreement number 101096021 (SUPERIOT, HORIZON-JU-SNS-2022-STREAM-B-01-03). T. Pinheiro acknowledges funding from FCT I.P. through the PhD Grant DFA/BD/8606/2020. J. C. also acknowledges the EMERGIA Junta de Andalucia program (EMC21_00174). M.S. and N.A. acknowledge São Paulo Research Foundation (FAPESP), Grant #2021/14141-1, Grant #2018/02604-4 and 2022/12332-7, Programa de Pós-graduação em Ciência e Tecnologia de Materiais (POSMAT), Coordenação de Aperfeiçoamento de Pessoal de Nível Superior (Capes), and Instituto Nacional de Eletrônica Orgânica (INEO).

Appendix A. Supplementary data

Supplementary data to this article can be found online at https://doi.org/10.1016/j.flatc.2024.100672.

References

[1] X. Zhang, C. Jiang, J. Liang, W. Wu, Electrode materials and device architecture strategies for flexible supercapacitors in wearable energy storage, J. Mater. Chem. A Mater. 9 (2021) 8099–8128, https://doi.org/10.1039/D0TA12299H.
[2] A. Khan, G. Grabher, G. Hossain, Smart-textile supercapacitor for wearable energy storage system, J. Energy Storage 73 (2023) 108963, https://doi.org/10.1016/J.EST.2023.108963.
[3] J. Lv, J. Chen, P.S. Lee, Sustainable wearable energy storage devices self-charged by human-body bioenergy, SusMat 1 (2021) 285–302, https://doi.org/10.1002/SUS2.14.
[4] J. Coelho, M.P. Kremer, S. Pinilla, V. Nicolosi, An outlook on printed microsupercapacitors: Technology status, remaining challenges, and opportunities, Curr. Opin. Electrochem. 21 (2020) 69–75, https://doi.org/10.1016/j.coelec.2019.12.004.
[5] R. Jia, G. Shen, F. Qu, D. Chen, Flexible on-chip micro-supercapacitors: Efficient power units for wearable electronics, Energy Storage Mater. 27 (2020) 169–186, https://doi.org/10.1016/j.ensm.2020.01.030.
[6] J. Zhao, A.F. Burke, Review on supercapacitors: Technologies and performance evaluation, J. Energy Chem. 59 (2021) 276–291, https://doi.org/10.1016/J.JECHEM.2020.11.013.
[7] D.P. Chatterjee, A.K. Nandi, A review on the recent advances in hybrid supercapacitors, J. Mater Chem. A Mater. 9 (2021) 15880–15918, https://doi.org/10.1039/D1TA02505H.
[8] T. Xu, Y. Wang, K. Liu, Q. Zhao, Q. Liang, M. Zhang, C. Si, Ultralight MXene/carbon nanotube composite aerogel for high-performance flexible supercapacitor, Adv Compos Hybrid Mater 6 (2023) 1–9, https://doi.org/10.1007/S42114-023-00675-8/FIGURES/5.
[9] F. Li, J. Qu, Y. Li, J. Wang, M. Zhu, L. Liu, J. Ge, S. Duan, T. Li, V.K. Bandari, M. Huang, F. Zhu, O.G. Schmidt, Stamping Fabrication of Flexible Planar Micro-Supercapacitors Using Porous Graphene Inks, Adv. Sci. 7 (2020) 2001561, https://doi.org/10.1002/advs.202001561.

[10] T. Pinheiro, S. Silvestre, J. Coelho, A.C. Marques, R. Martins, M.G.F. Sales, E. Fortunato, Laser-Induced Graphene on Paper toward Efficient Fabrication of FlexiblCe, Planar Electrodes for Electrochemical Sensing, Adv. Mater. Interfaces 8 (2021) 2101502, https://doi.org/10.1002/admi.202101502.
[11] R. Ye, D.K. James, J.M. Tour, Laser-Induced Graphene: From Discovery to Translation, Adv. Mater. 31 (2019) 1–15, https://doi.org/10.1002/adma.201803621.
[12] B. Kulyk, B.F.R. Silva, A.F. Carvalho, S. Silvestre, A.J.S. Fernandes, R. Martins, E. Fortunato, F.M. Costa, Laser-Induced Graphene from Paper for Mechanical Sensing, ACS Appl. Mater. Interfaces 13 (2021) 10210–10221, https://doi.org/10.1021/acsami.0c20270.
[13] L. Shan, Y. Zhang, Y. Xu, M. Gao, T. Xu, C. Si, Wood-based hierarchical porous nitrogen-doped carbon/manganese dioxide composite electrode materials for high-rate supercapacitor, Adv Compos Hybrid Mater 6 (2023) 1–10, https://doi.org/10.1007/S42114-023-00744-Y/FIGURES/6.
[14] J. Coelho, R.F. Correia, S. Silvestre, T. Pinheiro, A.C. Marques, M.R.P. Correia, J. V. Pinto, E. Fortunato, R. Martins, Paper-based laser-induced graphene for sustainable and flexible microsupercapacitor applications, Microchim. Acta 190 (2023) 1–10, https://doi.org/10.1007/s00604-022-05610-0.
[15] R. Correia, J. Deuermeier, M.R. Correia, J. Vaz Pinto, J. Coelho, E. Fortunato, R. Martins, Biocompatible Parylene-C Laser-Induced Graphene Electrodes for Microsupercapacitor Applications, ACS Appl. Mater. Interfaces 14 (2022) 46427–46438, https://doi.org/10.1021/acsami.2c09667.
[16] S.L. Silvestre, T. Pinheiro, A.C. Marques, J. Deuermeier, J. Coelho, R. Martins, L. Pereira, E. Fortunato, Cork derived laser-induced graphene for sustainable green electronics, Flexible Printed Electron. 7 (2022) 035021, https://doi.org/10.1088/2058-8585/ac8e7b.
[17] S. Wang, Y. Yu, S. Luo, X. Cheng, G. Feng, Y. Zhang, Z. Wu, G. Compagnini, J. Pooran, A. Hu, All-solid-state supercapacitors from natural lignin-based composite film by laser direct writing, Appl. Phys. Lett. 115 (2019), https://doi.org/10.1063/1.5118340.
[18] W. Qu, Z. Zhao, J. Wang, F. Dong, H. Xu, X. Sun, H. Jin, Direct laser writing of pure lignin on carbon cloth for highly flexible supercapacitors with enhanced areal capacitance, Sustain, Energy Fuels 5 (2021) 3744–3754, https://doi.org/10.1039/D1SE00828E.
[19] R. Ye, D.K. James, J.M. Tour, Laser-Induced Graphene, Acc. Chem. Res. 51 (2018) 1609–1620, https://doi.org/10.1021/acs.accounts.8b00084.
[20] S.-C. Pang, M.A. Anderson, T.W. Chapman, Novel Electrode Materials for Thin-Film Ultracapacitors: Comparison of Electrochemical Properties of Sol-Gel-Derived and Electrodeposited Manganese Dioxide, J. Electrochem. Soc. 147 (2000) 444, https://doi.org/10.1149/1.1393216.
[21] M. Toupin, T. Brousse, D. Bélanger, Influence of microstucture on the charge storage properties of chemically synthesized manganese dioxide, Chem. Mater. 14 (2002) 3946–3952, https://doi.org/10.1021/CM020408Q/SUPPL_FILE/CM020408Q_S.PDF.
[22] S.-L. Kuo, N.-L. Wu, Investigation of Pseudocapacitive Charge-Storage Reaction of MnO[sub 2]·nH[sub 2]O Supercapacitors in Aqueous Electrolytes, J. Electrochem. Soc. 153 (2006) A1317, https://doi.org/10.1149/1.2197667/XML.
[23] F. Béguin, E. Frackowiak, Supercapacitors: Materials, Systems, and Applications, Supercapacitors: Materials, Systems, and Applications (2013). doi: 10.1002/9783527646661.
[24] C. Zhu, X. Dong, X. Mei, M. Gao, K. Wang, D. Zhao, Direct laser writing of MnO2 decorated graphene as flexible supercapacitor electrodes, J. Mater. Sci. 55 (2020) 17108–17119, https://doi.org/10.1007/s10853-020-05212-2.
[25] J. Yao, L. Liu, S. Zhang, L. Wu, J. Tang, Y. Qiu, S. Huang, H. Wu, L. Fan, Metal-incorporated laser-induced graphene for high performance supercapacitors, Electrochim. Acta 441 (2023) 141719, https://doi.org/10.1016/J.ELECTACTA.2022.141719.
[26] R. Xu, Z. Wang, L. Gao, S. Wang, J. Zhao, Effective design of MnO2 nanoparticles embedded in laser-induced graphene as shape-controllable electrodes for flexible planar microsupercapacitors, Appl. Surf. Sci. 571 (2022) 151385, https://doi.org/10.1016/J.APSUSC.2021.151385.
[27] A. Vashisth, M. Kowalik, J.C. Gerringer, C. Ashraf, A.C.T. Van Duin, M.J. Green, ReaxFF Simulations of Laser-Induced Graphene (LIG) Formation for Multifunctional Polymer Nanocomposites, ACS Appl Nano Mater 3 (2020) 1881–1890, https://doi.org/10.1021/ACSANM.9B02524/ASSET/IMAGES/MEDIUM/AN9B02524_M003.GIF.
[28] H.W. Chang, Y.R. Lu, J.L. Chen, C.L. Chen, J.F. Lee, J.M. Chen, Y.C. Tsai, P.H. Yeh, W.C. Chou, C.L. Dong, Electrochemical and in situ X-ray spectroscopic studies of MnO2/reduced graphene oxide nanocomposites as a supercapacitor, PCCP 18 (2016) 18705–18718, https://doi.org/10.1039/C6CP01192F.
[29] M. Huang, Y. Zhang, F. Li, Z. Wang, N. Alamusi, Z. Hu, Q.L. Wen, Merging of Kirkendall growth and Ostwald ripening: CuO@MnO2 core-shell architectures for asymmetric supercapacitors, Sci Rep 4 (2014), https://doi.org/10.1038/SREP04518.
[30] M.C. Biesinger, B.P. Payne, A.P. Grosvenor, L.W.M. Lau, A.R. Gerson, R.S.C. Smart, Resolving surface chemical states in XPS analysis of first row transition metals, oxides and hydroxides: Cr, Mn, Fe, Co and Ni, Appl. Surf. Sci. 257 (2011) 2717–2730, https://doi.org/10.1016/J.APSUSC.2010.10.051.
[31] L. Lu, D. Zhang, Y. Xie, W. Wang, A stretchable, high-voltage and biobased microsupercapacitor using laser induced graphene/MnOx electrodes on cotton cloth, J Energy Storage 51 (2022) 104458, https://doi.org/10.1016/J.EST.2022.104458.
[32] A.C. Ferrari, Raman spectroscopy of graphene and graphite: Disorder, electron-phonon coupling, doping and nonadiabatic effects, Solid State Commun. 143 (2007) 47–57, https://doi.org/10.1016/j.ssc.2007.03.052.
[33] A.C. Ferrari, D.M. Basko, Raman spectroscopy as a versatile tool for studying the properties of graphene, Nat. Nanotechnol. 8 (2013) 235–246, https://doi.org/10.1038/nnano.2013.46.
[34] F. Bonaccorso, A. Lombardo, T. Hasan, Z. Sun, L. Colombo, A.C. Ferrari, Production and processing of graphene and 2d crystals, Materials Today 15 (2012) 564–589, https://doi.org/10.1016/S1369-7021(13)70014-2.
[35] A. Ogata, S. Komaba, R. Baddour-Hadjean, J.P. Pereira-Ramos, N. Kumagai, Doping effects on structure and electrode performance of K-birnessite-type manganese dioxides for rechargeable lithium battery, Electrochim. Acta 53 (2008) 3084–3093, https://doi.org/10.1016/J.ELECTACTA.2007.11.038.
[36] B. Xu, S. Yue, Z. Sui, X. Zhang, S. Hou, G. Cao, Y. Yang, What is the choice for supercapacitors: Graphene or graphene oxide?, Energy, Environ. Sci. 4 (2011) 2826–2830, https://doi.org/10.1039/c1ee01198g.
[37] N.H.N. Azman, M.S. Mamat @ Mat Nazir, L.H. Ngee, Y. Sulaiman, Graphene-based ternary composites for supercapacitors, Int J Energy Res 42 (2018) 2104–2116. doi: 10.1002/ER.4001.
[38] V. Naresh, N. Lee, A review on biosensors and recent development of nanostructured materials-enabled biosensors, Sensors (switzerland) 21 (2021) 1–35, https://doi.org/10.3390/s21041109.
[39] S. Bai, Y. Tang, Y. Wu, J. Liu, H. Liu, W. Yuan, L. Lu, W. Mai, H. Li, Y. Xie, High Voltage Microsupercapacitors Fabricated and Assembled by Laser Carving, ACS Appl. Mater. Interfaces 12 (2020) 45541–45548, https://doi.org/10.1021/acsami.0c11935.
[40] N. devi, M. Goswami, M. Saraf, B. Singh, S.M. Mobin, R.K. Singh, A.K. Srivastava, S. Kumar, Physicochemical and electrochemical behaviours of manganese oxide electrodes for supercapacitor application, J Energy Storage 28 (2020) 101228. doi: 10.1016/J.EST.2020.101228.
[41] C. Ma, Z. Li, J. Li, Q. Fan, L. Wu, J. Shi, Y. Song, Lignin-based hierarchical porous carbon nanofiber films with superior performance in supercapacitors, Appl. Surf. Sci. 456 (2018) 568–576, https://doi.org/10.1016/j.apsusc.2018.06.189.
[42] F. Mahmood, F. Mahmood, H. Zhang, J. Lin, C. Wan, Laser-Induced Graphene Derived from Kraft Lignin for Flexible Supercapacitors, ACS Omega 5 (2020) 14611–14618, https://doi.org/10.1021/acsomega.0c01293.
[43] J. Castro-Gutiérrez, A. Celzard, V. Fierro, Energy Storage in Supercapacitors: Focus on Tannin-Derived Carbon Electrodes, Front. Mater. 7 (2020) 560362, https://doi.org/10.3389/FMATS.2020.00217/BIBTEX.
[44] M. Diantoro, I. Istiqomah, Y. Al Fath, N. Nasikhudin, Y. Alias, W. Meevasana, Potential of MnO2-based composite and numerous morphological for enhancing supercapacitors performance, Int J Appl Ceram Technol 20 (2023) 2077–2098. doi: 10.1111/IJAC.14377.
[45] C. Hsiao, C. Lee, N. Tai, High retention supercapacitors using carbon nanomaterials/iron oxide/nickel-iron layered double hydroxides as electrodes, J Energy Storage 46 (2022) 103805, https://doi.org/10.1016/J.EST.2021.103805.
[46] H. Gul, A. ul H.A. Shah, S. Bilal, Achieving Ultrahigh Cycling Stability and Extended Potential Window for Supercapacitors through Asymmetric Combination of Conductive Polymer Nanocomposite and Activated Carbon, Polymers 2019, Vol. 11, Page 1678 11 (2019) 1678. doi: 10.3390/POLYM11101678.
[47] C. (John) Zhang, M. Liang, S.H. Park, Z. Lin, A. Seral-Ascaso, L. Wang, A. Pakdel, C. Coileaín, J. Boland, O. Ronan, N. McEvoy, B. Lu, Y. Wang, Y. Xia, J.N. Coleman, V. Nicolosi, Extra lithium-ion storage capacity enabled by liquid-phase exfoliated indium selenide nanosheets conductive network, Energy Environ Sci 13 (2020) 2124–2133. doi: 10.1039/D0EE01052A.
[48] C. (John) Zhang, L. McKeon, M.P. Kremer, S.H. Park, O. Ronan, A. Seral-Ascaso, S. Barwich, C. Coileáin, N. McEvoy, H.C. Nerl, B. Anasori, J.N. Coleman, Y. Gogotsi, V. Nicolosi, Additive-free MXene inks and direct printing of micro-supercapacitors, Nat Commun 10 (2019) 1–9. doi: 10.1038/s41467-019-09398-1.
[49] C. Zequine, C.K. Ranaweera, Z. Wang, S. Singh, P. Tripathi, O.N. Srivastava, B.K. Gupta, K. Ramasamy, P.K. Kahol, P.R. Dvornic, R.K. Gupta, High Per formance and Flexible Supercapacitors based on Carbonized Bamboo Fibers for Wide Temperature Applications, Scientific Reports 2016 6:1 6 (2016) 1–10. doi: 10.1038/srep31704.
[50] M. Reina, A. Scalia, G. Auxilia, M. Fontana, F. Bella, S. Ferrero, A. Lamberti, M. Reina, A. Scalia, G. Auxilia, M. Fontana, F. Bella, S. Ferrero, A.L. Politecnico, D. Torino, A. Lamberti, Boosting Electric Double Layer Capacitance in Laser-Induced Graphene-Based Supercapacitors, Adv Sustain Syst 6 (2022) 2100228, https://doi.org/10.1002/ADSU.202100228.
[51] P. Zaccagnini, D. di Giovanni, M.G. Gomez, S. Passerini, A. Varzi, A. Lamberti, Flexible and high temperature supercapacitor based on laser-induced graphene electrodes and ionic liquid electrolyte, a de-rated voltage analysis, Electrochim. Acta 357 (2020) 136838, https://doi.org/10.1016/J.ELECTACTA.2020.136838.
[52] Y. Ko, M. Kwon, W.K. Bae, B. Lee, S.W. Lee, J. Cho, Flexible supercapacitor electrodes based on real metal-like cellulose papers/639/4077/4079/4105/639/301/299/1013 article, Nat. Commun. 8 (2017) 1–11, https://doi.org/10.1038/s41467-017-00550-3.
[53] J. Li, Y. Shao, Q. Shi, C. Hou, Q. Zhang, Y. Li, R.B. Kaner, H. Wang, Calligraphy-inspired brush written foldable supercapacitors, Nano Energy 38 (2017) 428–437, https://doi.org/10.1016/j.nanoen.2017.06.013.
[54] H. Tariq, S.U. Awan, D. Hussain, S. Rizwan, S.A. Shah, S. Zainab, M.B. Riaz, Enhancing supercapacitor performance through design optimization of laser-

induced graphene and MWCNT coatings for flexible and portable energy storage, Scientific Reports 2023 13:1 13 (2023) 1–13. doi: 10.1038/s41598-023-48518-2.

[55] A. Lamberti, F. Clerici, M. Fontana, L. Scaltrito, A highly stretchable supercapacitor using laser-induced graphene electrodes onto elastomeric substrate, Adv. Energy Mater. 6 (2016) 1600050, https://doi.org/10.1002/aenm.201600050.

[56] X. Sun, X. Liu, X. Xing, F. Li, Electrodeposited with FeOOH and MnO2 on laser-induced graphene for multi-assembly supercapacitors, J. Alloy. Compd. 893 (2022) 162230, https://doi.org/10.1016/j.jallcom.2021.162230.